Japanese Journal of Applied Physics **50** (2011) 055802 **REGULAR PAPER**
DOI: 10.1143/JJAP.50.055802

Effect of $K_{0.5}Na_{0.5}NbO_3$ on Properties at and off the Morphotropic Phase Boundary in $Bi_{0.5}Na_{0.5}TiO_3$–$Bi_{0.5}K_{0.5}TiO_3$ Ceramics

Eva-Maria Anton, Wook Jo*, Joe Trodahl[1], Dragan Damjanovic[2], and Jürgen Rödel

Institute of Materials Science, Technische Universität Darmstadt, 64287 Darmstadt, Germany
[1]*MacDiarmid Institute of Advanced Materials and Nanotechnology, Victoria University, PO Box 600, Wellington, New Zealand*
[2]*Ceramics Laboratory, EPFL-Swiss Federal Institute of Technology, Lausanne 1015, Switzerland*

Received November 17, 2010; revised February 17, 2011; accepted February 28, 2011; published online May 20, 2011

Lead-free $(1-y)(Bi_{1/2}Na_{1/2}TiO_3$–$xBi_{1/2}K_{1/2}TiO_3)$–$yK_{0.5}Na_{0.5}NbO_3$ [$(1-y)$(BNT–xBKT)–yKNN] ($0.1 \le x \le 0.6$ and $0 \le y \le 0.05$) ceramics were prepared with compositions both at as well as off the morphotropic phase boundary (MPB) of $x = 0.2$ and $y = 0$. It was found that KNN addition destabilizes a ferroelectric order in BNT–BKT at zero electric-field, resulting in low remanent polarization, remanent strain and effective small signal $d_{33,eff}$ [23 pC/N for $(x, y) = (0.2, 0.05)$, 60 pC/N for $(0.2, 0.02)$], while it does not affect the maximum polarisation and strain at high fields and thus enhances large signal piezoelectric coefficient, d_{33}* [200 pm/V for $(0.2, 0.05)$, 217 pm/V for $(0.2, 0.02)$]. This effect of KNN was found to be independent from the MPB and thus equally high d_{33}* values were obtained for compositions at and far off the MPB. Thus, adding KNN to BNT–BKT removes the restriction to remain at exactly MPB position and provides more flexibility while offering equal or even improved strain.

1. Introduction

$Pb(Zr,Ti)O_3$ (PZT) and its derivatives have dominated the piezoelectric market for most applications over more than half a century.[1,2] However, growing awareness of the hazardous effect of lead on environment and human health initiated intensive research on lead-free piezoceramics, mainly focusing on alkali-niobate- and bismuth-based perovskites.[3] Legislation in the European Union banned the use of lead and other heavy metals in electric and electronic devices starting from 2006.[4] Similar laws were enforced in other industrial countries all over the world.[5–10] However, in the EU and other countries exemption for the use of lead in piezoceramics was granted as long as there is no suitable alternative available. In order to replace lead with environmentally friendly alternatives, lead-free end members with different phases were combined in order to form a morphotropic phase boundary (MPB) similar to that in PZT, e.g., in $Bi_{1/2}Na_{1/2}TiO_3$–$0.06BaTiO_3$ (BNT–0.06BT)[11] and $Bi_{1/2}Na_{1/2}TiO_3$–$0.2Bi_{1/2}K_{1/2}TiO_3$ (BNT–0.2BKT).[12,13] Like in PZT, enhanced properties with respect to piezoelectric coefficient, electromechanical coupling factor and field-induced strain were obtained in the lead-free MPB systems. However, the enhanced properties in most piezoceramics are only found in a very narrow range of compositions. Therefore small differences in stoichiometry could result in a large discrepancy in properties. This is most likely one of the reasons why the exact position of the MPB reported in literature for these materials differs.[14,15] In BNT–BT, the MPB is usually found between 6 and 8 mol % BT,[11,16–18] and in BNT–BKT peak values in properties are found between 16 and 20 mol % BKT.[12,19–21] It follows that a range of compositions is usually found in the literature as MPB composition.

The reproducibility of materials has been attended to as one of the most critical challenges. Deviations in stoichiometry are known to be caused by the hygroscopic nature of the elements in the starting powders, which could result in errors in weighing, or loss of the volatile elements like Bi, Na, and K.[22,23] In $(K_{0.5}Na_{0.5})NbO_3$ (KNN)-based systems, it was found that the volatility of alkali metals can be efficiently suppressed by sintering in closed crucibles.[24] In BNT–BT[25] and BNT–BKT[23,26] systems, excess Bi was shown to improve properties significantly, serving as compensation for Bi loss during processing. Adding 1 mol % of Bi excess to BNT–BKT lead to improved properties and a shift in MPB up to 20–24 mol % BKT.[26] This indicates that there might not only be compensation for Bi loss, but more mechanisms involved. For example, B-site vacancies due to excess Bi, which may improve domain wall mobility, or increased density owing to excess Bi acting as a sintering aid were proposed.[26–28] A similar effect of improved properties due to non-stoichiometry was observed in BNT–BT.[18,29] Overall it becomes apparent that stoichiometry requires precise control during processing to find reproducible, intrinsic material properties or to introduce well defined deviations from the stoichiometric composition.

In addition, in bismuth–alkaline metal based lead-free systems, the temperature limit for application, the depolarisation temperature T_d, is lowest for MPB compositions.[11,20] Thus it is desirable to find lead-free alternatives which show good performance independent from an MPB. So far only little research was done on ferroelectric and piezoelectric properties of BNT–xBKT above $x = 0.3$, mainly pointing out few compositions and properties.[12,30] Yoshii *et al.*[13] explored piezoelectric properties of BNT–xBKT up to $x = 0.5$, but did not provide strain or polarisation data for $x > 0.3$. In this work piezoelectric and ferroelectric properties of BNT–xBKT were investigated in a broad compositional range and the effect of KNN addition at the MPB as well as away from the MPB was explored. At the MPB of BNT–BKT, an earlier work reported an enhanced large-signal d_{33}* for 1 mol % 0.97KNN–0.03BKT addition.[31] In the current work it was shown that KNN improves the large-signal d_{33}* for a wide range of compositions. Moreover, strain behaviour was found to be almost independent from the composition for (BNT–xBKT)–0.05KNN, which widens the processing window and improves reproducibility of properties.

2. Experimental Procedure

$(1-y)(Bi_{1/2}Na_{1/2}TiO_3$–$xBi_{1/2}K_{1/2}TiO_3)$–$yK_{0.5}Na_{0.5}NbO_3$ [$(1-y)$(BNT–xBKT)–yKNN] with $0.1 \le x \le 0.6$ and

*E-mail address: jo@ceramics.tu-darmstadt.de

$0 \leq y \leq 0.05$ were prepared by the conventional solid state reaction method. Note that these compositions are different to those published in previous work,[31] where 0.97KNN–0.03BKT was added to BNT–BKT. Starting powders Bi_2O_3 (99.975%, Alfa Aesar), Na_2CO_3 (99.5%, Alfa Aesar), K_2CO_3, (99.0%, Alfa Aesar), Nb_2O_5 (99.9%, Alfa Aesar), and TiO_2 (99.9%, Alfa Aesar) were weighed according to the respective stoichiometry, taking into account the impurities of the raw powders. Special attention was paid to maintaining stoichiometry as exact as possible during all processing steps. To prevent adsorption of water, the hygroscopic K_2CO_3 was weighed in dry argon atmosphere in a glove box. The powder mixture was planetary-milled (Fritsch) with zirconia balls in ethanol for 24 h at 250 rpm. House-made, fully organic nylon milling containers were used in order to avoid possible contamination during the milling process. Milled powders were dried, ground and calcined in closed alumina crucibles at 800 °C for 5 h with a heating rate of 5 °C/min. Milling was repeated for the calcined powders under the same conditions as for the raw powder mixture. Dried and ground powders were lightly compacted into disc shaped pellets, cold isostatically pressed at 350 MPa and sintered in closed alumina crucibles at 1060–1100 °C for 3 h depending on composition. Samples were embedded in atmospheric powder of the same composition to prevent possible evaporation of volatile elements during sintering.

X-ray diffraction (XRD) patterns from calcined powders (Stoe Stadi P, Cu $K\alpha_1$) and sintered samples (Bruker D3 Advance, Cu $K\alpha$) revealed a single phase perovskite structure. Lattice parameters were refined by a Rietveld method using FullProf software to calculate the theoretical density. In order to check the quality of the processing, inductively coupled plasma optical emission spectrometry (ICP-OES) measurements were performed for selected samples (InfraServ), which showed no deviation from the intended stoichiometry within accuracy of the measurement. Scanning electron microscopy (SEM) images (Philips/FEI L30 FEG/ESEM) of polished and thermally etched surfaces were used to determine the average grain size by a linear intercept method. Density was measured by Archimedes method. Raman spectra were collected at room temperature using 488 nm excitation with a Jobin-Yvon LabRam HR800 (Horiba). Spectra were corrected with a white light calibration curve.

For electrical measurements disc shaped samples were ground to a thickness less than 1 mm so that the diameter was ~10 times larger than thickness. Samples were sputtered with silver electrodes on both faces. Unipolar and bipolar strain using an optical sensor (Philtec) and polarisation were measured in a Sawyer–Tower circuit at a maximum triangular-shaped electric field of 6 kV/mm at the frequency of 1 Hz. Samples were poled in a silicon oil bath at room temperature with a dc electric field of 5 kV/mm for 10 min to 1 h. Planar coupling factors k_p were determined on these poled samples using serial and parallel resonance frequencies obtained by an impedance analyzer (HP 4194A). An effective small signal piezoelectric coefficient $d_{33,eff}$ was measured at 200 Hz on the same poled disc shaped samples using a home-made Berlincourt meter type d_{33} meter.

Table I. Relative densities (%) for $(1 - y)$(BNT–xBKT)–yKNN.

y	x					
	0.1	0.2	0.3	0.4	0.5	0.6
0.05	95.9	96.4	95.6	94.5	95.7	97.5
0.02	98.5	97.6	96.0	93.8	93.9	91.6
0	97.2	95.0	95.2	96.3	97.1	96.2

Table II. Average grain sizes (μm) for $(1 - y)$(BNT–xBKT)–yKNN.

y	x					
	0.1	0.2	0.3	0.4	0.5	0.6
0.05	0.6	0.4	0.4	0.4	0.4	0.4
0.02	0.5	0.4	0.4	0.4	0.4	0.3
0	0.7	0.4	0.4	0.4	0.3	0.5

3. Results and Discussion

Relative densities of all compositions obtained from Archimedes method are presented in Table I. The density of most samples is higher than 95% of the relative density. For 2 mol % KNN samples with $x \geq 0.4$, however, only lower relative densities between 91.6 and 93.9% could be achieved with normal sintering. The average grain size was 0.4 ± 0.1 μm and very similar for all compositions, as provided in Table II. Only grains in samples with $x = 0.1$ are slightly larger with 0.6 ± 0.1 μm.

Figure 1 displays XRD profiles of sintered samples at room temperature. Note that the data were collected with a laboratory X-ray source and thus might not represent the true structure of the bulk material, which could be different from the surface diffraction patterns.[32] Figures 1(a) and 1(b) present XRD patterns for BNT–xBKT. In $x = 0.1$ and 0.2, the apparent splitting in the $(111)_{pc}$ (the subscript "pc" refers to pseudocubic index) reflection indicates a rhombohedral structure. For $x = 0.2$ additional splitting in the $(200)_{pc}$ reflection implies that this composition contains a mixed phase of rhombohedral and tetragonal structure. In all patterns with $x > 0.2$ there is no evidence for a peak splitting in the $(111)_{pc}$ reflection but in the $(200)_{pc}$ reflection, indicating a single tetragonal distortion in the unit cell. These results agree well with earlier X-ray studies, which proposed a morphotropic phase boundary with mixed rhombohedral and tetragonal phase around $x = 0.2$.[12,19,20] Figures 1(c) and 1(d) show that the structure also changes with increasing KNN content for $x = 0.1$. The apparent splitting in the $(111)_{pc}$, which characterizes a rhombohedral distortion, is no longer observed when $y = 0.05$. At the current stage, however, it is not clear whether the disappearance of rhombohedral symmetry is due to insufficient resolution of the equipment or due to a change in the symmetry.

To further investigate the structural transitions, Raman spectroscopy was performed at room temperature. Figure 2(a) presents Raman spectra for BNT–xBKT samples without KNN. The patterns change from $x = 0.1$ to 0.2; this is visible from a softening and weakening of the soft mode near 130 cm^{-1}, a broadening of the mode near 280 cm^{-1} and a hardening of the mode near 590 cm^{-1} by 30

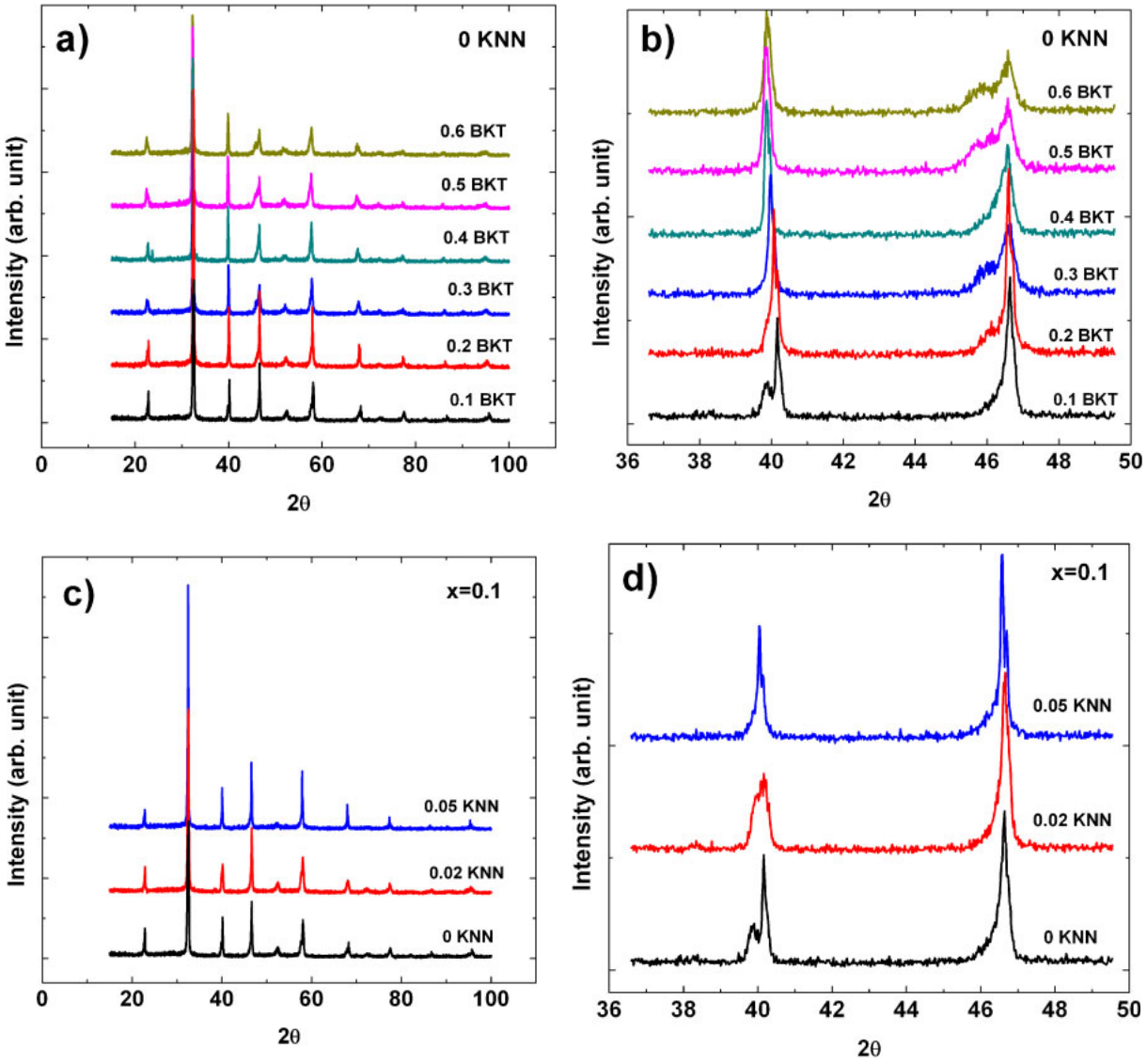

Fig. 1. (Color online) XRD profiles of BNT–xBKT with increasing x (a) for the entire 2θ range, and (b) a selected angular range to magnify $(111)_{pc}$ and $(200)_{pc}$ reflections. XRD profiles of $(1-y)$(BNT–0.1BKT)–yKNN with increasing y (c) for the entire 2θ range, and (d) a selected angular range to magnify $(111)_{pc}$ and $(200)_{pc}$ reflections.

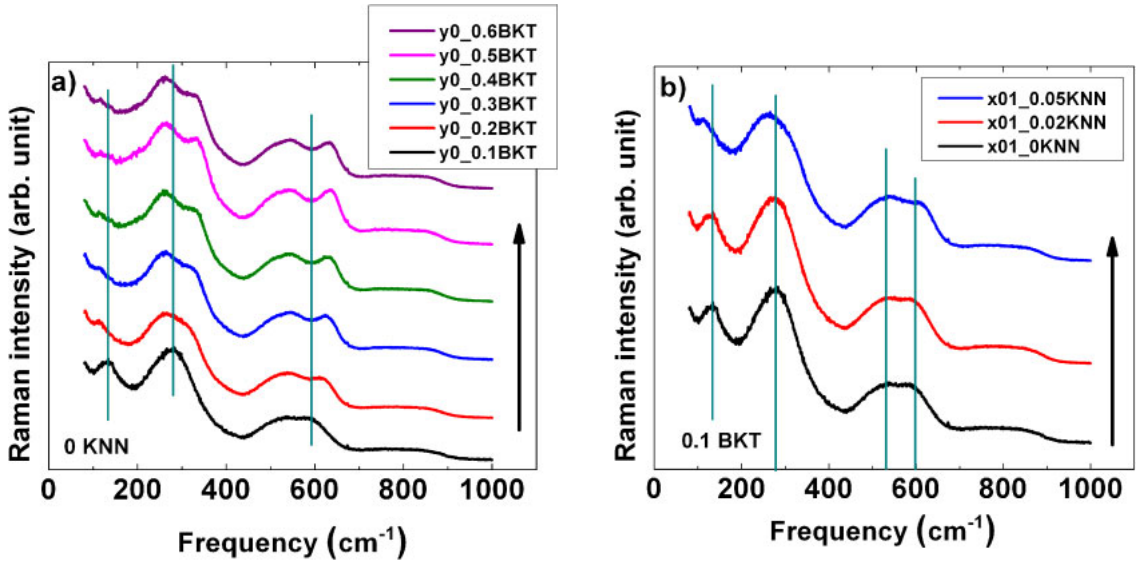

Fig. 2. (Color online) Room temperature Raman spectra for $(1-y)$(BNT–xBKT)–yKNN; increasing content in (a) BKT or (b) KNN is marked by arrow.

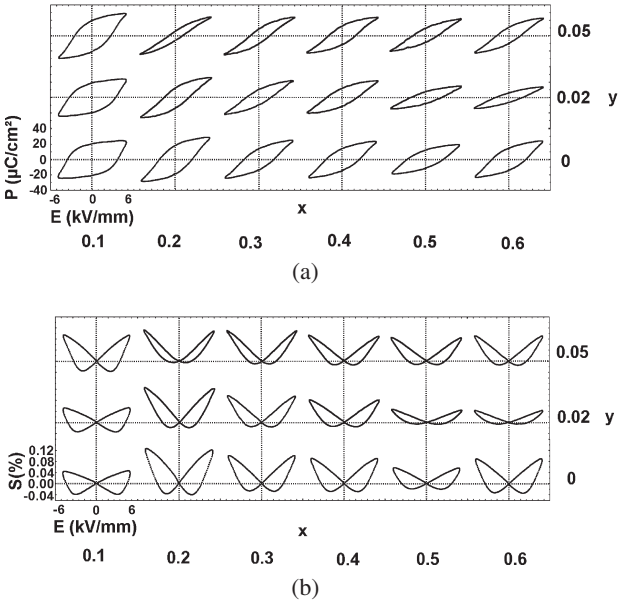

Fig. 3. (a) Bipolar polarisation and (b) bipolar strain for $(1-y)$(BNT–xBKT)–yKNN samples at a maximum electric field of 6 kV/mm and 1 Hz frequency.

cm^{-1}. Between $x = 0.2$ and 0.3 the 280 cm^{-1} mode splits into a 270 and a 320 cm^{-1} mode, which is accompanied by a further softening and weakening of the soft mode and a hardening of the high frequency mode from 620 to 630 cm^{-1}. The spectra change little, and only gradually for higher BKT content. A reasonable interpretation is that a structural transition takes place between $x = 0.1$ to 0.3, with a mixed phase at $x = 0.2$. This transition across $x \approx 0.2$ agrees well with the results from X-ray studies,[12,19,20] where a mixed rhombohedral and tetragonal phase is observed near BNT–0.2BKT. In contrast, previous Raman studies by Kreisel *et al.*[33] on crushed BNT–BKT single crystals reported a discontinuous change in the spectra at $x = 0.4$.

Figure 2(b) shows the Raman spectra for $x = 0.1$ with different KNN concentrations. Comparing 0 mol % KNN and 2 mol % KNN compositions reveals no difference in the modes, but a significant change of the modes can be found at 5 mol % KNN composition, which resembles the mixed-phase spectrum of the $(x, y) = (0.2, 0)$ sample. The similarities between the Raman spectra suggest that a line assuming a mixed phase connects the compositions $(0.2, 0)$, $(0.2, 0.02)$, and $(0.1, 0.05)$. It is interesting to note that the Raman spectra for $(0.1, 0.05)$ and $(0.2, 0)$ are almost identical, while XRD profiles are completely different. This suggests that KNN may destabilize rhombohedral symmetry favoring tetragonal as BKT does and additionally destroys a long-range symmetry of the system. The loss of long range coherence would affect XRD but not Raman spectra. The Raman spectra for the remaining samples, i.e., all those for which $x > 0.2$ and even for $x = 0.2$ with $y > 0.0$ display practically the same pattern implying that they all have a tetragonal symmetry.

It is interesting to compare this pattern to the Raman data reported for BNT–BT.[34–36] In that system the transition occurs near 6 mol % BT, but with spectra that change exactly as we found here, with the 130 cm^{-1} mode softening and weakening, the 280 cm^{-1} mode splitting and the high frequency mode hardening. There is a clear and strong resemblance between these systems.

Figure 3(a) provides bipolar polarisation loops for $(1-y)$(BNT–xBKT)–yKNN ceramics with $0.1 \leq x \leq 0.6$ and $0 \leq y \leq 0.05$. The remanent polarisation P_r and maximum polarisation P_{max} are summarized in Figs. 4(a) and 4(b), respectively. For samples on the BNT-rich side of the MPB ($x = 0.1$), the coercive field E_c and P_r are relatively high (~4 kV/mm and ~20 μC/cm^2, respectively), with P_r being almost as high as P_{max} (~23 μC/cm^2). The square shape of the polarisation loops for 0 and 2 mol % KNN is similar to those of pure BNT.[1] Only E_c of the 5 mol % KNN containing sample is comparably small (3 kV/mm), while P_r compared to 0 and 2 mol % compositions stays practically constant and P_{max} increases to 29 μC/cm^2, leading to a stretched ferroelectric shape fairly similar to that of the MPB samples. These results agree well with the observations from the Raman spectra in Fig. 2, showing a phase transition between 2 and 5 mol % KNN, which was assumed to be a transition from rhombohedral into an MPB-like phase mixture.

For samples without KNN at the MPB and on the BKT-rich side of the MPB ferroelectric polarisation loops with E_c of about 3 kV/mm are obtained. P_r generally decreases for higher BKT contents. Two anomalies are observed, one is the well-known high P_{max} (29 μC/cm^2) at the MPB. The other is found at $x = 0.6$, revealing an unexpected increase of P_{max} and P_r for this composition. As mentioned earlier, many studies on the structure of BNT–BKT were done, often giving controversial results presumably arising from difficult sample preparation, especially for single crystals, and the very small distortions from the cubic cell.[12,33,37–41] Elkechai *et al.*[38] performed XRD studies on polycrystalline samples which showed a biphasic region from $x = 0.2$ to 0.6. Although the proposed structures might not be correct, it gave a clue that there could be another phase transition around $x = 0.6$, which is consistent with the currently observed abrupt increase in P_{max} and P_r in this sample.

The effect of KNN on ferroelectric properties of BNT–BKT is found to lower E_c and P_r significantly. The narrowest loop with a very small P_r (6 μC/cm^2) is found at $x = 0.2$ at the highest KNN percentage ($y = 0.05$). P_{max}, on the other hand, is not significantly changed among the samples without KNN or with a lower KNN content. In 2 mol % KNN samples with $x = 0.5$ and 0.6, polarisation does not show a typical ferroelectric behaviour. In these samples E_c might be higher than the applied electric field or the ferroelectric contribution is too small to be visible. The altered shape of the curves with increasing KNN content can be explained by the evolution of a ferroelectric phase with small P_r at room temperature. By applying an electric field, ferroelectric phase with large P_r can be induced easily due to similar free energy compared to the phase with low P_r, and thus P_{max} is equally high as in unmodified ferroelectric samples.[42]

The effect of KNN on BNT–BKT becomes more evident from the bipolar strain curves in Fig. 3(b). Samples on the BNT-rich side of the MPB ($x = 0.1$) show a ferroelectric strain loop with low total strains and almost equal amounts of positive and negative strain, similar to BNT.[43] As expected from the higher P_{max} and the assumed mixed

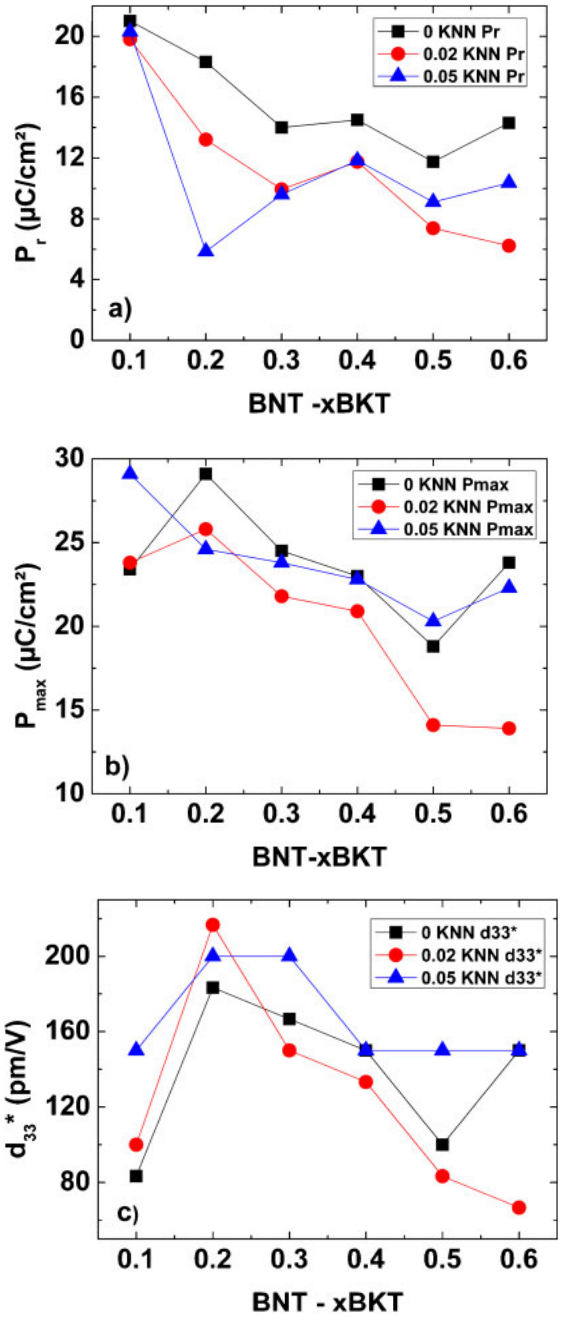

Fig. 4. (Color online) Bipolar (a) remanent polarisation P_r, (b) maximum polarisation P_{max}, and (c) unipolar large signal $d_{33}{}^*$ of $(1-y)$(BNT–xBKT)–yKNN ceramics.

phase, for the 5 mol % KNN composition, higher total strain is observed compared to the samples with 0 or 2 mol % KNN.[44)]

The anomalous behaviour at $x = 0.6$ for samples without KNN is also observed in the strain behaviour, resulting in comparably high total strain. The highest total strain is found at the MPB, while the lowest strains are found in $(0.5, 0.02)$ and $(0.6, 0.02)$ that are samples with low remanent polarisation. With increasing amount of KNN, less negative strain is observed, changing the character of the curves from those typical for a "normal" ferroelectric to those showing mainly the characteristics of the quadratic electrostrictive behaviour.[45)] The electrostrictive-like behaviour is most pronounced in $(0.2, 0.05)$, which is in agreement with the

Table III. Depolarisation temperature (°C) for $(1-y)$(BNT–xBKT)–yKNN.

y	x					
	0.1	0.2	0.3	0.4	0.5	0.6
0.05	67	113	100	120	98	93
0.02	137	97	120	207	180	218
0	194	153	236	253	265	246

results from polarisation measurements. For 0 and 2 mol % KNN, strain varies significantly for different BNT/BKT ratios, whereas in 5 mol % KNN compositions almost the same total strain is found for the whole range of BNT/BKT ratios. This can be explained by a combined effect of electrically induced ferroelectric order[42)] and electrostrictive strain, which is independent from the position of the MPB. One of the biggest advantages of the observed MPB-independent enhanced properties is good reproducibility. This is particularly pertinent for these materials given the critical issues in the processing of lead-free ferroelectrics.[14–16)] An important issue to be noted is that the maximum achieved strains in this work (e.g., 0.16% for BNT–0.2BKT at 6 kV/mm, bipolar) are smaller than those reported in literature for BNT–BKT with 0.23% (8 kV/mm, unipolar),[13)] BNT–BKT–KNN with 0.46% (8 kV/mm, bipolar)[31)] and Nb-doped BNT–BKT with 0.45% (7 kV/mm, unipolar).[46)] It is assumed that the large strain behaviour in BNT–BKT–(KNN) could be partly due to a non-stoichiometry arising from the underestimated mass of the hygroscopic ingredients, which may lead to an enhanced polarisation as compared to stoichiometric samples.[18,26)]

The depolarisation temperature T_d of all the investigated compositions is tabulated in Table III. Details of the methods on how T_d is determined can be found in ref. 47. It is known that KNN decreases T_d in BNT–BT.[45,48)] A similar behaviour is confirmed in BNT–BKT. Both 5 mol % KNN compositions at the MPB and on the BKT-rich side of the MPB lose their polarisation state at about 100 °C, whereas in BNT–BKT without or with 2 mol % KNN T_d varies from 150 °C at the MPB to more than 260 °C away from the MPB. Since KNN lowers T_d, the samples with increasing KNN get closer to the transition temperature, eventually rendering only the high-temperature low-P_r ferroelectric phase stable at room temperature without applied electric field.

Figure 4(c) presents large signal $d_{33}{}^*$ values ($d_{33}{}^* = S_{max}/E_{max}$) based on unipolar strain data not shown here. In conformity to the literature, the $d_{33}{}^*$ has its peak at the MPB (183 pm/V) in the case of KNN-free compositions and as expected from the bipolar strain curves, the 2% KNN compositions also have highest values of $d_{33}{}^*$ at the MPB (217 pm/V). However, for the compositions with 5% KNN content, this MPB-induced maximum gets less pronounced and the highest value (200 pm/V) is found equally at $x = 0.2$ and 0.3. This is consistent with the observations in Fig. 3, where the strain was found to vary little with different BKT contents. It implies that for the compositions with KNN, the temperature-dependent polymorphism is more important than the composition-dependent polymorphism (i.e., MPB) in enhancing the functional properties.

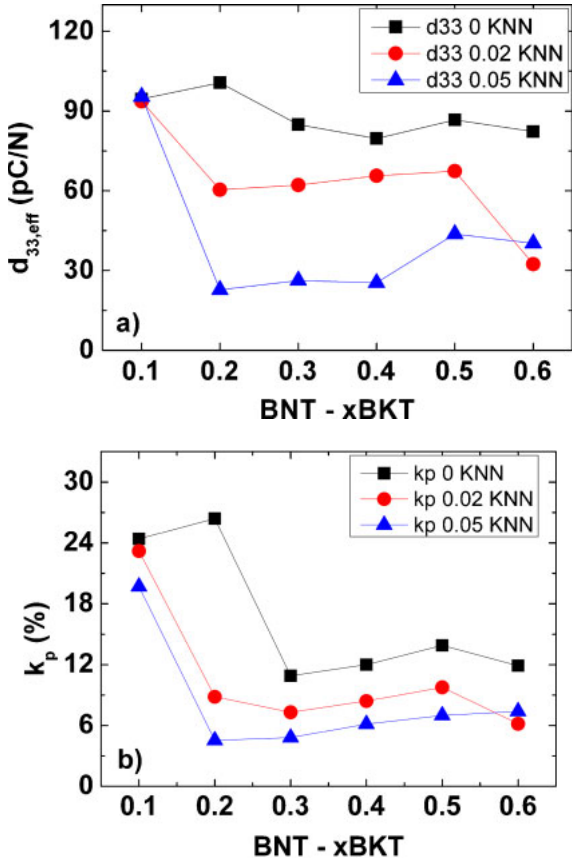

Fig. 5. (Color online) (a) $d_{33,eff}$ and (b) k_p of room temperature poled $(1-y)$(BNT–xBKT)–yKNN ceramics.

Effective small signal piezoelectric coefficient $d_{33,eff}$ and planar electromechanical coupling factor k_p are provided in Fig. 5. For the compositions without KNN $d_{33,eff}$ and k_p increase from BNT–0.1BKT ($d_{33,eff} = 95\,pC/N$, $k_p = 24\%$) compared to the MPB composition ($d_{33,eff} = 101\,pC/N$, $k_p = 26\%$). For $x > 0.2$ both material coefficients drop and stay nearly at the same level for all higher BKT-contents. For the 2 and 5% KNN compositions $d_{33,eff}$ and k_p are highest on the BNT-rich side of the MPB, decrease for $x = 0.2$ ($d_{33,eff} = 23\,pC/N$ and $k_p = 4.5\%$ for $y = 0.05$) and then also remain nearly at the same level for higher BKT contents. For all compositions with $x \geq 0.2$ both $d_{33,eff}$ and k_p decrease with increasing KNN content. This is expected from the reduced remanent polarisation with increasing KNN as shown in Fig. 4(a). A low remanent polarization means that only low poling and thus low small signal properties are achievable, which is due to the reduced ferroelectric order at zero electric field for higher KNN contents. Nevertheless, the large signal value for samples with KNN $d_{33}{}^*$ is even higher than that in the samples without KNN, as demonstrated in Fig. 4(c). This can be explained by an electric-field induced phase with higher remanent polarization, whose free energy is close to the phase with low P_r. Thus, despite the low small signal properties, enhanced $d_{33}{}^*$ as well as high bipolar strains are observed in KNN containing samples due to the high-P_r phase induced by the large applied electric fields together with the electrostrictive effect.

4. Conclusions

Lead-free $(1-y)$(BNT–xBKT)–yKNN ($0.1 \leq x \leq 0.6$ and $0 \leq y \leq 0.05$) samples were investigated with respect to their structural and ferroelectric properties dependent on the composition with respect to the MPB and KNN content. Comparison between Raman and XRD data suggest that KNN destabilizes rhombohedral symmetry favoring tetragonal structure and as well destroys the long-range symmetry of the system. It was found that KNN weakens ferroelectric order in BNT–BKT. Thus remanent polarisation and remanent strain are decreased while maximum polarisation and strain remain at the level of pure BNT–BKT, since ferroelectric order can easily be induced in those samples. As a result of low remanent polarisation samples cannot be poled efficiently and $d_{33,eff}$ and k_p are small compared to pure BNT–BKT. Large signal $d_{33}{}^*$ on the other hand is highest for 0.05 KNN samples. This effect of KNN is independent from the distance to the MPB, thus equally high strains can be achieved at and far off the MPB, making processing and reproducibility easier.

Acknowledgement

This work was supported by the state center AdRIA on adaptronics.

1) B. Jaffe, W. R. Cook, and H. Jaffe: *Piezoelectric Ceramics* (Academic Press, London, 1971) Vol. 1.
2) G. H. Haertling: J. Am. Ceram. Soc. **82** (1999) 797.
3) J. Rödel, W. Jo, K. T. P. Seifert, E.-M. Anton, T. Granzow, and D. Damjanovic: J. Am. Ceram. Soc. **92** (2009) 1153.
4) EU-Directive 2002/95/EC: Restriction of the use of certain hazardous substances in electrical and electronic equipment (RoHS): Offic. J. European Union **46** (2003) 19.
5) Solid waste: hazardous electronic waste: U.S. California Senate Bill No. 20 (2003).
6) Solid waste: hazardous electronic waste: U.S. California Senate Bill No. 50 (2004).
7) Act for Resource Recycling of Electrical and Electronic Equipment and Vehicles: Environment and Labor Committee of the National Assembly of Korea, Bill Nr. 6319 (2007).
8) Measures for the Administration on Pollution Control of Electronic Information Products: Ministry of Information Industry China Order No. 39 (2006).
9) Law for promotion of effective utilization of resources: Minister of Economy, Trade and Industry, Japan (2001).
10) The marking for presence of the specific chemical substances for electrical and electronic equipment: Japan Electronics and Information Technology Industries Association (2005) JIS C 0950.
11) T. Takenaka, K. Maruyama, and K. Sakata: Jpn. J. Appl. Phys. **30** (1991) 2236.
12) A. Sasaki, T. Chiba, Y. Mamiya, and E. Otsuki: Jpn. J. Appl. Phys. **38** (1999) 5564.
13) K. Yoshii, Y. Hiruma, H. Nagata, and T. Takenaka: Jpn. J. Appl. Phys. **45** (2006) 4493.
14) S. E. Park, S. J. Chung, I. T. Kim, and K. S. Hong: J. Am. Ceram. Soc. **77** (1994) 2641.
15) S. E. Park and K. S. Hong: J. Appl. Phys. **79** (1996) 383.
16) M. Chen, Q. Xu, B. H. Kim, B. K. Ahn, J. H. Ko, W. J. Kang, and O. J. Nam: J. Eur. Ceram. Soc. **28** (2008) 843.
17) C. Xu, D. Lin, and K. W. Kwok: Solid State Sci. **10** (2008) 934.
18) B. J. Chu, D. R. Chen, G. R. Li, and Q. R. Yin: J. Eur. Ceram. Soc. **22** (2002) 2115.
19) Z. Yang, B. Liu, L. Wei, and Y. Hou: Mater. Res. Bull. **43** (2008) 81.
20) Y. Hiruma, K. Yoshii, H. Nagata, and T. Takenaka: J. Appl. Phys. **103** (2008) 084121.
21) W. Zhao, H. P. Zhou, Y. K. Yan, and D. Liu: Key Eng. Mater. **368–372** (2008) 1908.

22) T. A. Skidmore and S. J. Milne: J. Mater. Res. **22** (2007) 2265.
23) H. Nagata, T. Shinya, Y. Hiruma, and T. Takenaka: in *Developments in Dielectric Materials and Electronic Devices*, ed. K. M. Nair (Wiley, New York, 2005) Ceramic Transactions, Vol. 167, p. 213.
24) Y. Wang, D. Damjanovic, N. Klein, and N. Setter: J. Am. Ceram. Soc. **91** (2008) 1962.
25) X. X. Wang, X. G. Tang, K. W. Kwok, H. L. W. Chan, and C. L. Choy: Appl. Phys. A **80** (2005) 1071.
26) Y. R. Zhang, J. F. Li, B. P. Zhang, and C. E. Peng: J. Appl. Phys. **103** (2008) 074109.
27) H. Du, D. Liu, F. Tang, D. Zhu, W. Zhou, and S. Qu: J. Am. Ceram. Soc. **90** (2007) 2824.
28) M. Zhu, L. Liu, Y. Hou, H. Wang, and H. Yan: J. Am. Ceram. Soc. **90** (2007) 120.
29) X. X. Wang, S. W. Or, X. G. Tang, H. L. W. Chan, P. K. Choy, and P. C. K. Liu: Solid State Commun. **134** (2005) 659.
30) S. C. Zhao, G. R. Li, A. L. Ding, T. B. Wang, and Q. R. Yin: J. Phys. D **39** (2006) 2277.
31) K. T. P. Seifert, W. Jo, and J. Rödel: J. Am. Ceram. Soc. **93** (2010) 1392.
32) W. Y. Chang, A. H. King, and K. J. Bowman: J. Mater. Res. **22** (2007) 2845.
33) J. Kreisel, A. M. Glazer, G. Jones, P. A. Thomas, L. Abello, and G. Lucazeau: J. Phys.: Condens. Matter **12** (2000) 3267.
34) D. Rout, K. S. Moon, V. S. Rao, and S. J. L. Kang: J. Ceram. Soc. Jpn. **117** (2009) 797.
35) S. Trujillo, J. Kreisel, Q. Jiang, J. H. Smith, P. A. Thomas, P. Bouvier, and F. Weiss: J. Phys.: Condens. Matter **17** (2005) 6587.
36) B. Wylie-van Eerd, D. Damjanovic, N. Klein, N. Setter, and J. Trodahl: Phys. Rev. B **82** (2010) 104112.
37) Y. Yamada, T. Akutsu, H. Asada, K. Nozawa, S. Hachiga, T. Kurosaki, O. Ikagawa, H. Fujiki, K. Hozumi, T. Kawamura, T. Amakawa, K. Hirota, and T. Ikeda: Jpn. J. Appl. Phys. **34** (1995) 5462.
38) O. Elkechai, M. Manier, and J. P. Mercurio: Phys. Status Solidi A **157** (1996) 499.
39) G. O. Jones, J. Kreisel, and P. A. Thomas: Powder Diffr. **17** (2002) 301.
40) G. O. Jones, J. Kreisel, V. Jennings, M. A. Geday, P. A. Thomas, and A. M. Glazer: Ferroelectrics **270** (2002) 191.
41) I. P. Pronin, N. N. Parfenova, N. V. Zaitseva, V. A. Isupov, and G. A. Smolensky: Sov. Phys. Solid State **24** (1982) 1060.
42) W. Jo, T. Granzow, E. Aulbach, J. Rodel, and D. Damjanovic: J. Appl. Phys. **105** (2009) 094102.
43) A. B. Kounga, S.-T. Zhang, W. Jo, T. Granzow, and J. Rödel: Appl. Phys. Lett. **92** (2008) 222902.
44) D. Damjanovic: Rep. Prog. Phys. **61** (1998) 1267.
45) S.-T. Zhang, A. B. Kounga, W. Jo, C. Jamin, K. Seifert, T. Granzow, J. Rödel, and D. Damjanovic: Adv. Mater. **21** (2009) 4716.
46) K.-N. Pham, A. Hussain, C. W. Ahn, I. W. Kim, S. J. Jeong, and J.-S. Lee: Mater. Lett. **64** (2010) 2219.
47) E.-M. Anton, W. Jo, D. Damjanovic, and J. Rödel: unpublished.
48) S. T. Zhang, A. B. Kounga, E. Aulbach, W. Jo, T. Granzow, H. Ehrenberg, and J. Rödel: J. Appl. Phys. **103** (2008) 034108.